A Study on the Piezoelectric Motor of High Actuating Force

Jwo Ming, Jou

Department of Mechanical Engineering, Cheng Shiu University
e-mail: joujm@csu.edu.tw

Abstract: This study is to investigate a new type piezoelectric motor of high actuating force, of which there are four different types design of the piezoelectric stator for the new type piezoelectric motor. And this new type piezoelectric motor has the advantages of high loading ability and low rotational speed. Wherein it net weight is only 40gw, but the loading ability can be up 590gw, as for rotational speed is no more than 53rpm under conditions of $180V_{p-p}$ driving voltage and 25.4kHz driving frequency. The new type piezoelectric motor is by an I-type stator, four multi-block piezoelectric ceramic sets and rotor composed. In addition, we found the best motion trajectory or vibration mode shape, driving ability and electromechanical physical behavior from the computer simulations and experiments. And we are also from the results of the simulation and experimental, reverse to estimate the approximate solution of all possible theoretical framework.
[Jwo Ming, Jou. **A Study on the Piezoelectric Motor of High Actuating Force.** *Life Sci J* 2013;10(2):242-248] (ISSN:1097-8135). http://www.lifesciencesite.com. 38

Keywords: High Actuating Force, Piezoelectric Motor, I-Type Stator, Multi-Block Piezoelectric Ceramic Sets, Rotor, Loading Ability, Rotational Speed.

1. Introduction

The advantage of traditional motor has a higher rotational speed, but the torque or loading is not large [1-5]. As for the rotational speed of piezoelectric motor is not the fastest, but there is having a higher torque or loading. In general, the piezoelectric motor of the kind can be divided into two, one is a translation type, and the other is a rotary type. Although their structure and mode of operation principle is different, but the ultimate purpose and application is the same. Among the translation-type piezoelectric motor can move fast on the platform. For example, the array or matrix type piezoelectric motor [6-10]. Among them, the maximum speed can be up to 286mm/s, while the maximum loading ability can reach 15kgw or 147.15N. And the translation-type piezoelectric motor can also be used to toggle the slider or the rotor. For example, the piezoelectric motor of the centipede type or long column type [11-16], among them, can make the moving speed on the rail up to 176.2mm/s [11-16], shown as Table I.

As for the piezoelectric motor of the rotary type, which are mainly the toggle slider moves or friction rotation of the rotor by the elliptical motion of the stator, or made rail cars, so that they can movement on tracks. For example, the form of the metal tubular piezoelectric motor or a multilayer piezoelectric motor [17-21]. Among them, the maximum speed and loading is 2200rpm and 495gw or 4.86N respectively.

Due to the different needs of the mechanical and electrical systems as well as limit the development of the patented technology, making the piezoelectric motor study also followed the change and innovation. The piezoelectric motor of high actuating force is a new design in this study. Its main feature is having the performance and efficacy of the low speed and high loading ability or high actuating force.

TABLE I. THE PERFORMANCE OF PRIOR PIEZOELECTRIC LINEAR MOTORS[11-16].

REFERENCE	DRIVING VOLTAGE (V_{P-P})	MAXIMUM SPEED (MM/S)	DRIVING FREQUENCY (KHZ)
PRUITTIKORN ET AL., 2012 [11]	60	176.2	28.2
LU ET AL., 2006 [12]	92	94.5	38.6
RHO ET AL., 2005 [13]	99	36.0	35.4
ROH AND KWON, 2004 [14]	100	62.0	28.6
ROH ET AL., 2001 [15]	100	40.0	23.5
HE ET AL., 1998 [16]	36	8.0	23.4

Composition and Operation Principle

In this study, the main components of the piezoelectric motor of high actuating force include: a stator, four multi-block piezoelectric ceramic sets, a spring, rotor, a bearing and a screw, shown as Figure1-2. Which the stator has a head part, body part and base part. And the inside of stator can accommodate a spring, shown as Figure3. The head part of the stator which is a short circular cylinder, which has a tapered hole inside. And the tapered hole with rotor to maintain the best contact. The body part

of the stator is a quartet. The quartet on the outside surface of the block can be separately installed multi-block piezoelectric ceramic set. The base part of the stator has a screw hole for tightening set screws for use, shown as Figure3. Assembly, the first multi-block piezoelectric ceramic set installed in the stator of the body part, and then set each set of spring, gear type rotor and bearing, and finally the use of locking screws all the components. Operation, we can respectively multi-block piezoelectric ceramic set is subject to different or the same resonant frequency, driving voltage and phase angle (as shown in Figure4), thereby to promote the high actuating force piezoelectric motor to drive the precision machinery systems or optical systems, shown as Figure5-6.

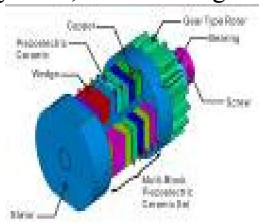

Figure 1: The isometric view of the piezoelectric motor of high actuating force.

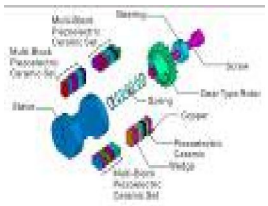

Figure 2: The exploded view of the piezoelectric motor of high actuating force.

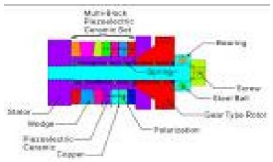

Figure 3: The profile view of the piezoelectric motor of high actuating force.

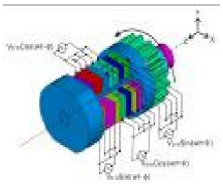

Figure 4: The operation principle of the piezoelectric motor of high actuating force.

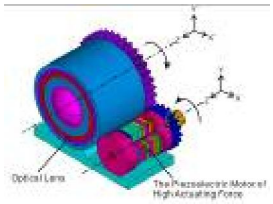

Figure 5: The application case of the piezoelectric motor of high actuating force (before the opening of the optical lens).

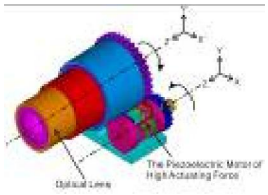

Figure 6: The application case of the piezoelectric motor of high actuating force (after the opening of the optical lens).

Constitutive Equations

We can understand the characteristics of the piezoelectric motor through the constitutive equation of d-form or e-form [22], as:

$$\{S\}_{6\times1} = [s]^{E}_{6\times6}\{T\}_{6\times1} + \{d\}_{6\times3}\{E\}_{3\times1}. \quad (1)$$

$$\{D\}_{3\times1} = \{d\}_{3\times6}\{T\}_{6\times1} + [\varepsilon]^{T}_{3\times3}\{E\}_{3\times1}. \quad (2)$$

or

$$\{T\}_{6\times1} = [c]^{E}_{6\times6}\{S\}_{6\times1} - \{e\}_{6\times3}\{E\}_{3\times1}. \quad (3)$$

$$\{D\}_{3\times1} = \{e\}_{3\times6}\{S\}_{6\times1} + [\varepsilon]^{S}_{3\times3}\{E\}_{3\times1}. \quad (4)$$

Where ***c, D, d, E, e, S, s*** and ***T*** represents the stiffness, electric displacement, piezoelectric strain constant, electric field, strain, flexible constant and stress separately. And ε represents the tensor of the permittivity. The superscript ***E, T*** and ***S*** represents constant electric field, constant tensor and constant strain separately.

However, in the present study, we are more concerned about the physical properties of piezoelectric ceramic [17], such as Table II.

TABLE II. THE PHYSICAL PROPERTIES OF PIEZOELECTRIC CERAMIC[17].

PHYSICAL NAME	PHYSICAL QUANTITIES
PIEZOELECTRIC STRAIN CONSTANTS	$d_{31} = d_{32} = -274$ (pm/V), $d_{33} = 593$ (pm/V) $d_{15} = d_{24} = 741$ (pm/V)
PERMITTIVITY	$\varepsilon_{11} = \varepsilon_{22} = 15.3$ (nF/m), $\varepsilon_{33} = 15.1$ (nF/m)
PIEZOELECTRIC STRESS CONSTANTS	$e_{31} = e_{32} = -5.3$ (N/Vm), $e_{33} = 15.8$ (pm/V) $e_{15} = e_{24} = 12.3$ (pm/V)
STIFFNESS CONSTANTS	$c_{11} = c_{22} = 120$ (GPa), $c_{33} = 111$ (GPa) $c_{44} = 30$ (GPa), $c_{55} = c_{66} = 26$ (GPa), $c_{12} = c_{21} = 75.2$ (GPa) $c_{13} = c_{31} = c_{23} = c_{32} = 75.1$ (GPa)
DENSITY	$\rho = 7{,}700$ (kg/m^3)

Equation of Motions

The present study describes the piezoelectric motor of high actuating force is a plane strain problem. That is the longitudinal strain can be ignored ($S_3 = S_4 = S_5 \approx 0$). Therefore, it is the equation of motion should be expressed as [17]:

$$\frac{\partial T_1}{\partial x} + \frac{\partial T_6}{\partial y} + \frac{\partial T_5}{\partial z} = \rho\frac{\partial^2 u}{\partial t^2}. \quad (5)$$

$$\frac{\partial T_6}{\partial x} + \frac{\partial T_2}{\partial y} + \frac{\partial T_4}{\partial z} = \rho\frac{\partial^2 v}{\partial t^2}. \quad (6)$$

$$\frac{\partial T_5}{\partial x} + \frac{\partial T_4}{\partial y} + \frac{\partial T_3}{\partial z} = \rho\frac{\partial^2 w}{\partial t^2}. \quad (7)$$

And

$$T_1 = c_{11}^E\left(\frac{\partial u}{\partial x} - z\frac{\partial^2 w}{\partial x^2}\right) + c_{12}^E\left(\frac{\partial v}{\partial y} - z\frac{\partial^2 w}{\partial y^2}\right) - e_{31}\frac{\partial \psi_3}{\partial z}. \quad (8)$$

$$T_2 = c_{12}^E\left(\frac{\partial u}{\partial x} - z\frac{\partial^2 w}{\partial x^2}\right) + c_{22}^E\left(\frac{\partial v}{\partial y} - z\frac{\partial^2 w}{\partial y^2}\right) - e_{32}\frac{\partial \psi_3}{\partial z}. \quad (9)$$

$$T_3 = c_{12}^E\left(\frac{\partial u}{\partial x} - z\frac{\partial^2 w}{\partial x^2}\right) + c_{12}^E\left(\frac{\partial v}{\partial y} - z\frac{\partial^2 w}{\partial y^2}\right) - e_{33}\frac{\partial \psi_3}{\partial z}. \quad (10)$$

$$T_4 = -e_{24}\frac{\partial \psi_2}{\partial y}. \quad (11)$$

$$T_5 = -e_{15}\frac{\partial \psi_1}{\partial x}. \quad (12)$$

$$T_6 = c_{66}^E\left(\frac{\partial v}{\partial x} + \frac{\partial u}{\partial y} - 2z\frac{\partial^2 w}{\partial x \partial y}\right). \quad (13)$$

Where ***u, v,*** and ***w*** represents the different direction of displacement separately. And c_{pq} and e_{ip} represents the tensor of the stiffness constants and piezoelectric stress constants separately.

According to the equation (1)~(13), we can assume or predict that the solid elliptical orbit of the piezoelectric stator or motor, such as:

$$\left(\frac{u}{U_m}\right)^2 + \left(\frac{v}{V_m}\right)^2 + \left(\frac{w}{W_m}\right)^2 = 1. \quad (14)$$

Where

$$u = U_m \sin(\omega_m t + \phi)\sin\omega_m t. \quad (15)$$

$$v = V_m \cos(\omega_m t + \phi)\sin\omega_m t. \quad (16)$$

$$w = W_m \cos\omega_m t. \quad (17)$$

And

$$U_m = c_{xi} d_{3i} V_{p-p}. \quad (18)$$

$$V_m = c_{yi} d_{3i} V_{p-p}. \quad (19)$$

$$W_m = c_{zi} d_{3i} V_{p-p}. \quad (20)$$

Where U_m, V_m and W_m represents the amplitude of the horizontal, vertical and longitudinal direction separately. $\omega_m(=2\pi f_m)$ represents driving angle velocity, where f_m representatives resonance frequency or driving frequency. And ϕ driving phase angle. Where c_{xi}, c_{yi} and c_{zi} represents horizontal, vertical and longitudinal direction out of revise coefficient tensor separately, and where *the subscript i=1, 2, 3.* d_{3i} represents piezoelectric strain constant of d-form. Such as d_{31}, d_{32} *and* d_{33}. Where $d_{31}=d_{32}$ *for PZT.* V_{p-p} represents driving voltage. And t represents driving time.

Therefore the different planes trajectory can be represented as:

(1) The trajectory in the xy plane:

$$\left(\frac{u}{U_m \sin\omega_m t}\right)^2 + \left(\frac{v}{V_m \sin\omega_m t}\right)^2 = 1. \quad (21)$$

(2) The trajectory in the yz plane:

$$\left(\frac{v}{V_m \cos(\omega_m t + \phi)}\right)^2 + \left(\frac{w}{W_m}\right)^2 = 1. \quad (22)$$

and

(3) The trajectory in the xz plane:

$$\left(\frac{u}{U_m \sin(\omega_m t + \phi)}\right)^2 + \left(\frac{w}{W_m}\right)^2 = 1. \quad (23)$$

For piezoelectric motor, based on previous studies [1-8], the importance of the xy plane trajectory or Eq.(21) is much higher than other plane trajectory or Eq.(22) and Eq.(23).

Simulation and Experiment

We chose four different types of piezoelectric stator to simulate in this study, shown as Figure 7-10 and Table III. Wherein the piezoelectric stator is composed by the I-type base, the piezoelectric ceramic slices and conductive copper slices. Due to thin conductive copper considerable, so the simulation, we choose to be ignored. As for the physical properties of the piezoelectric ceramic slices are obtained as shown in Table II. The base material is selected 6061 type of aluminum alloy. And its density, Young's modulus and Poisson ratio is 2,700kg/m^3, 70GPa and 0.3.

We use the Ansys code and the solid 98 element type of coupled field to simulate for all materials. To save the computer simulation computation time for piezoelectric stator, we choose the smart size 9 to mesh. In order to meet the need of the actual assembly and experimental, we set the mechanical and electrical boundary condition for the Fixed-Free and open circuit separately.

In this experiment, the main component contains the piezoelectric stators and rotor, pins and mass, the physical properties shown as Table III, Table IV and s Figure 11-12.

In this experiment, we use the power amplifier (Model: A-303, A.A. Lab. Systems Ltd. Co.) and dual channel arbitrary function generator (Model:AFG-3022, Tektronix Co.) to drive the piezoelectric motor and use the digital tachometer (Model:RM-1501, TES Electrical Electronic Co.) to measure the rotational speed of the rotor (gear) under different driving conditions.

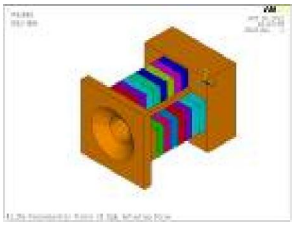

Figure 7: #1 piezoelectric stator.

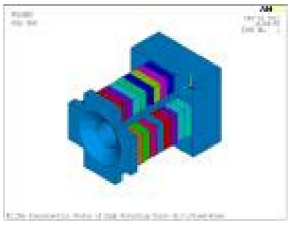

Figure 8: #2 piezoelectric stator.

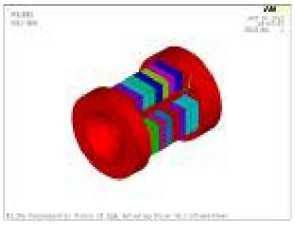

Figure 9: #3 piezoelectric stator.

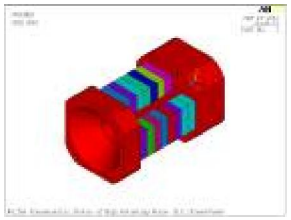

Figure10: #4 piezoelectric stator.

Figure 11: The different type stator of the piezoelectric motor of high actuating force.

Figure 12: The composition and testing mass of the piezoelectric motor of high actuating force.

Figure 13: The experimental structure of piezoelectric motor of high actuating force.

Figure 14: The experimental structure of testing rotational speed and loading ability.

TABLE III. THE NET WEIGHT AND SIZE OF PIEZOELECTRIC STATORS

TYPE	NET WEIGHT (GW)	SIZE (MM)
#1	29.9	18 X 18 X 26
#2	29.5	18 X 18 X 26
#3	31.8	18 X 18 X 26.5
#4	30.2	18 X 18 X 29

TABLE IV. THE PHYSICAL PROPERTIES OF THE MAIN COMPONENTS OF PIEZOELECTRIC MOTOR

ITEM	NET WEIGHT (GW)	SIZE (MM)
ROTOR	12.0	OD20, ID6, T1
PIN OF ROTOR	0.4	D2, L20
MASS	53.0	OD50, ID6.1, T10
PIN OF MASS	1.4	D2, L50

IV. RESULTS AND DISCUSSION

According to the results of simulations and experiments, we found:

(1) Under condition of different smart sizes, we found the number of elements and computing time, there are clearly different, it is found that the resonance frequency and the amount of deformation of the respective mode shape very close, Shown as Table V.

(2) Under the same smart size and electromechanical boundary conditions, the maximum deformation or trajectory occurs in the fourth mode shape of different type piezoelectric stator, Shown as Table V and Figure 15-18.

(3) Under the same smart size and electromechanical boundary conditions, the maximum deformation or trajectory occurs in the first mode shape of different type piezoelectric stator on xy-plane, shown as Table VI and Figure 19-22.

(4) Under the $180V_{p-p}$ driving voltage, 25.4kHz optimal resonance frequency and 90^0 driving phase angle conditions, the maximum rotational speed is 53rpm for #1 piezoelectric motor, shown as Figure 23.

(5) Under the $180V_{p-p}$ driving voltage, 23.1kHz optimal resonance frequency and 0^0 driving phase angle conditions, the maximum rotational speed is 44rpm for #2 piezoelectric motor, shown as Figure 23.

(6) Under the $180V_{p-p}$ driving voltage, 22.5kHz optimal resonance frequency and 150^0 driving phase angle conditions, the maximum rotational speed is 41rpm for #3 piezoelectric motor, shown as Figure 23.

(7) Under the $180V_{p-p}$ driving voltage, 20.4kHz optimal resonance frequency and 0^0 driving phase angle conditions, the maximum rotational speed is 22rpm for #4 piezoelectric motor, shown as Figure 23.

(8) Under the $180V_{p-p}$ driving voltage, 25.4kHz optimal resonance frequency and 0^0 driving phase angle conditions, the maximum rotational speed is 45rpm for #1 piezoelectric motor, shown as Figure 24.

(9) Under the $180V_{p-p}$ driving voltage, 23.1kHz

optimal resonance frequency and 0^0 driving phase angle conditions, the maximum rotational speed is 44rpm for #2 piezoelectric motor, shown as Figure 24.

(10) Under the $180V_{p-p}$ driving voltage, 22.5kHz optimal resonance frequency and 0^0 driving phase angle conditions, the maximum rotational speed is 38rpm for #3 piezoelectric motor, shown as Figure 24.

(11) Under the $180V_{p-p}$ driving voltage, 20.4kHz optimal resonance frequency and 0^0 driving phase angle conditions, the maximum rotational speed is 22rpm for #4 piezoelectric motor, shown as Figure 24.

(12) Under the $180V_{p-p}$ driving voltage, 0^0 driving phase angle and net weight conditions, the #1 piezoelectric motor driving bandwidth is from 22.1kHz to 27.1kHz, shown as Figure 24.

(13) Under the $180V_{p-p}$ driving voltage, 0^0 driving phase angle and net weight conditions, the #2 piezoelectric motor driving bandwidth is from 21.0kHz to 24.3kHz, shown as Figure 24.

(14) Under the $180V_{p-p}$ driving voltage, 0^0 driving phase angle and net weight conditions, the #3 piezoelectric motor driving bandwidth is from 20.4kHz to 23.8kHz, shown as Figure 24.

(15) Under the $180V_{p-p}$ driving voltage, 0^0 driving phase angle and net weight conditions, the #1 piezoelectric motor driving bandwidth is from 20.4kHz to 22.1kHz, shown as Figure 24.

(16) Under conditions of 0^0 driving phase angle, optimal resonance frequency, 140Vp-p average driving voltage and net weight, the maximum average rotational speed is 42.4rpm, 35.8rpm, 28.9rpm and 14.8rpm of #1, #3, #2 and #4 piezoelectric motor separately, shown as Figure 25.

(17) Under conditions of 0^0 driving phase angle, optimal resonance frequency, 180Vp-p driving voltage and 305gw average loading, the maximum average rotational speed is 37.1rpm, 30.7rpm, 29.4rpm and 15.0rpm of #1, #2, #3 and #4 piezoelectric motor separately, shown as Figure 26.

TABLE V. THE 1ST AND 2ND MODE FREQUENCY AND DEFORMATION OF #1 PIEZOELECTRIC STATOR UNDER CONDITION OF DIFFERENT SMART SIZES.

ITERM / SMART SIZE	10	9	8	7
ELEMENT NUMBER	3,804	4,071	4,263	5,407
COMPUTING TIME (SEC)	30	35	54	65
1ST MODE FREQUENCY (KHZ)	24.114	24.135	23.951	23.994
2ND MODE FREQUENCY (KHZ)	37.208	37.257	36.895	37.057
1ST MODE DOFORMATION (M/M)	20.308	20.335	20.251	20.305
2ND MODE DOFORMATION (M/M)	13.422	13.976	14.027	13.903

TABLE VI. THE MAXIMUN DEFORMATION OF THE FIRST FOUR MODES OF DIFFERENT TYPES PIEZOELECTRIC STATOR.

TYPE & MODE	FIXED-FREE(KHZ)	RXYZ(M/M)	RXY(M/M)	RYZ(M/M)	RZX(M/M)
#1-1	**24.1**	20.3	**20.3**	14.5	14.5
#1-2	37.3	14.0	2.6	14.0	14.0
#1-3	45.0	29.3	11.0	29.2	27.3
#1-4	**48.7**	**37.1**	12.9	35.2	37.0
#2-1	**25.4**	16.2	**20.6**	14.7	14.7
#2-2	37.9	9.1	2.8	9.2	9.1
#2-3	47.1	14.9	8.8	15.0	12.2
#2-4	**51.9**	**16.5**	9.8	13.6	16.7
#3-1	**22.1**	14.5	**20.5**	14.6	14.6
#3-2	33.2	9.6	2.8	9.1	9.0
#3-3	40.7	14.4	8.3	14.4	12.2
#3-4	**45.4**	**16.3**	9.4	13.6	16.4
#4-1	**22.7**	14.8	**17.9**	12.8	12.7
#4-2	36.7	9.6	4.2	9.7	9.5
#4-3	42.7	16.8	11.7	16.8	12.5
#4-4	**46.2**	**18.6**	12.7	14.2	18.6

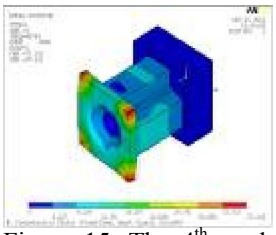

Figure 15: The 4th mode shape of #1 piezoelectric stator.

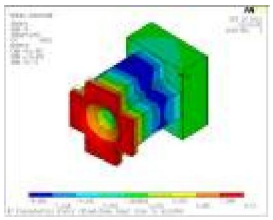

Figure 16: The 4th mode shape of #2 piezoelectric stator.

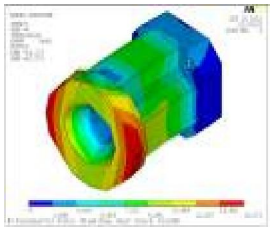

Figure 17: The 4th mode shape of #3 piezoelectric stator.

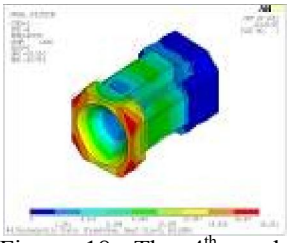

Figure 18: The 4th mode shape of #4 piezoelectric stator.

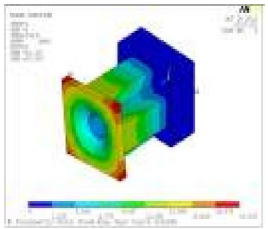

Figure 19: The 1st mode shape of #1 piezoelectric stator.

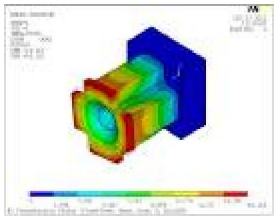

Figure 20: The 1st mode shape of #1 piezoelectric stator.

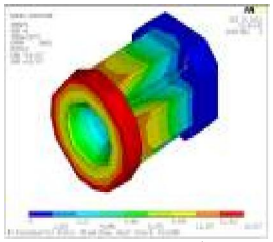

Figure 21: The 1st mode shape of #1 piezoelectric stator.

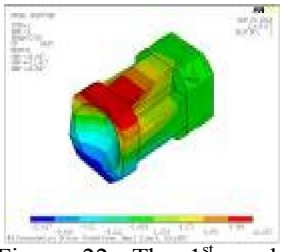

Figure 22: The 1st mode shape of #1 piezoelectric stator.

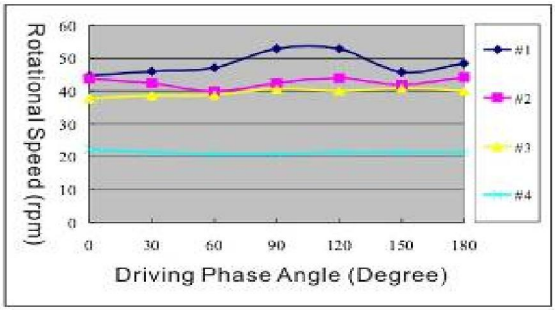

Figure 23. The rotational speed relative to the driving phase angle of #1~#4 piezoelectric motor under conditions of $180V_{p-p}$ driving voltage and net weight.

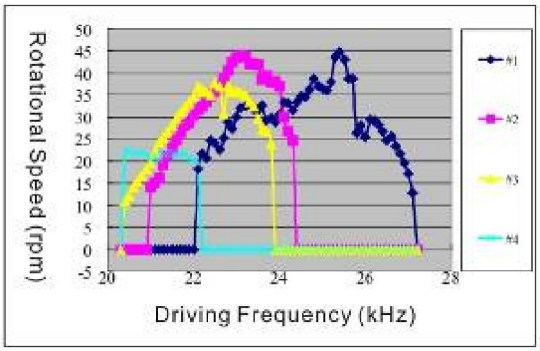

Figure 24. The movement speed relative to the driving frequency of #1~#4 piezoelectric motor under conditions of different driving ways and $180V_{p-p}$ driving voltage.

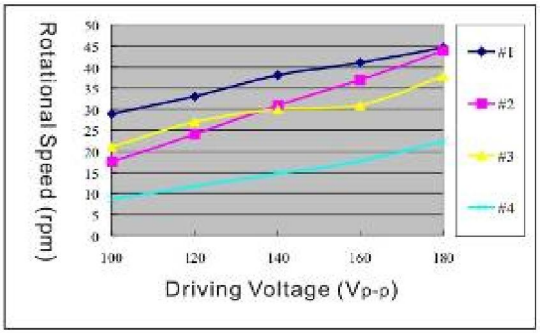

Figure 25. The rotational speed relative to the driving voltage of #1~#4 piezoelectric motor under conditions of 0^0 driving phase angle and optimal resonance frequency.

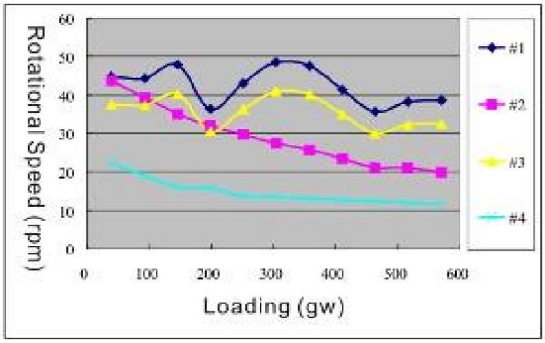

Figure 26. The movement speed relative to the loading under conditions of different driving ways and $180V_{p-p}$ driving voltage.

V. CONCLUSION

In this study, we found the fourth vibration modal vibration displacement is much larger than the other vibration modes from the results of computer simulations by Ansys code. However, in the experiment, they found the best driving ability of the first vibration mode. This particular physical phenomena, we can find a reasonable explanation from the analysis of the results of the computer simulation. The main reason is the first vibration mode on the xy-plane vibration displacement is much higher than other vibration

modes and the other plane. In other words, the xy-plane vibration displacement decided piezoelectric motor driving ability, including rotational speed and loading ability. In addition, we also found the piezoelectric motor loading ability is much higher than previously studied piezoelectric motor. Of course, we also found that the piezoelectric motor speed is very low. That is, the type of piezoelectric motor is suitable for the use of low-speed electrical and mechanical systems. From the experiments of different types of piezoelectric motor, we also found that the piezoelectric stator lip is continuity and a relatively thin, its ability to drive will be better. If the piezoelectric the lip portion of the stator belong to the non-continuous, and its driving ability is relatively poor.

Acknowledgement

This study can be finished smoothly, we should thank for NSC of Taiwan, ROC (Plan No.:NSC101-2221-E-230-002).

References

[1] G. Murugananth, S. Vijayan and S. Muthukrishnan, "**Analysis of Various Anti-Windup Schemes used to Control PMDC Motors employed in Orthopedic Surgical Simulators**", Life Science Journal, Vol.10, No.1, pp.226-230 (2013).

[2] Mehdi Akbarpour, Saeed Zakrei, Mohammad Lohi, Mohammad Amin Zakrei and Mohammad Masoud Mirjalili, "**Indirect Vector Control of Induction Motor by Adjusting PI Parameter Using Genetic Algorithm**", Life Science Journal, Vol.10, No.1, pp.431-437 (2013).

[3] Eman M Khedr, Noha Abo El Fetoh, Hosam Khalifa, Mohamed A Ahmed and Khaled M A El Beh, "**Prevalence of Depression, Anxiety, Dementia and other Non Motor Features of a large Cohort of Egyptian Parkinson's Disease Patients**", Life Science Journal, Vol.09, No.2, pp.509-518 (2012).

[4] Ananthamoorthy. N.P and Baskaran. K, "**Performance Analysis of PMSM Drive Using Intelligent Hybrid Fuzzy Controller**", Life Science Journal, Vol.09, No.1, pp.112-120 (2012).

[5] Fawzia El Sayed Abusaad and Mohammed Ali Kassem, "**The Effect of Nursing Intervention on Eliminating Feeding Problems induced by Deficit Oral-Motor function mong Children with Severe Head Injury**", Life Science Journal, Vol.09, No.3, pp.475-383 (2012).

[6] Jwo-Ming Jou, "**A Study on the Arch Type Ultrasonic Motor**", International Conference on Electric Information and Control Engineering, ICEICE 2011, IEEE publication, pp.1123-1126 (2011/04/15-17, Wuhan of China).

[7] Jwo-Ming Jou, "**A Study on the Crab Type Ultrasonic Motor**", 5th International Symposium in Science and Technology at Cheng Shiu University 2010, pp.49-53 (2010/08/24-25, Kaohsiung of Taiwan).

[8] Jwo-Ming Jou, Huang-Kuang Kung and Bo-Wun Huang, "**A Study on the Square Matrix Type Ultrasonic Motor**", 2009 International Symposium on Mechatronic and Biomedical Engineering & Applications, pp.247-252 (2009/11/05, Kaohsiung of Taiwan).

[9] J. M. Jou and J. L. Hou, "**A Study on the New Type Linear Ultrasonic Motor**", 2007 IEEE International Ultrasonic Symposium, pp. 2554-2557 (2007, New York of USA).

[10] Jwo-Ming, Jou and Wei-Shiang, Shu, "**A Study for the Pillar Array Type Piezoelectric Motor**", 2006 Taiwan-Russia Research Cooperation Symposium, pp171-177 (2006/11/072007, Kaohsiung of Taiwan).

[11] Pruittikorn Smithmaitrie, Panumas Suybangdum, Pitak Laoratanakul, and Nantakan Muensit, "Design and Performance Ttesting of an Ultrasonic Linear Motor with Dual Piezoelectric Actuators", IEEE Transactions on Ultrasonics, Ferroelectrics, and Frequency Control, Vol. 59, No. 5 , pp.1033-1042 (May 2012).

[12] C . Lu, T. Xie, T. Zhou, and Y. Chen, "Study of a New Type Linear Ultrasonic Motor with Double-Driving Feet", Ultrasonics, Vol. 44, Suppl.1 , pp.e585–e589 (2006).

[13] J. S. Rho, B. J. Kim, C. H. Lee, H. W. Joo, and H. K. Jung, "Design and Characteristic Analysis of L1B4 Ultrasonic Motor Considering Contact Mechanism," IEEE Trans. Ultrason. Ferroelectr. Freq. Control, vol. 52, no. 11, pp. 2054–2064, 2005.

[14] Y. Roh and J. Kwon, "Development of a New Standing Wave Type Ultrasonic Linear Motor," Sens. Actuators A, Vol. 112, No. 2–3, pp.196–202 (2004).

[15] Y. Roh, S. Lee, and W. Han, "Design and Fabrication of a New Traveling Wave-Type Ultrasonic Linear Motor," Sens. Actuators A, Vol. 94, No. 3, pp. 205–210 (2001).

[16] S . He, W. Chen, X. Tao, and Z. Chen, "Standing Wave Bi-Directional Linearly Moving Ultrasonic Motor," IEEE Trans. Ultrason. Ferroelectr. Freq. Control, Vol. 45, No. 5, pp. 1133–1139 (1998).

[17] Jwo-Ming Jou, "**A Study on the H Type Piezoelectric car**", International Conference on Electric Information and Control Engineering, ICEICE 2012, IEEE publication, pp.4261-4264 (2012/04/06-08, Lushan of China).

[18] Jwo-Ming Jou, "**A Study on the Multi-Block Piezoelectric car**", 2011 International Symposium on Mechatronic and Biomedical Engineering & Applications, pp.123-128 (2011/11/08, Taiwan, Republic of China).

[19] J. M. Jou, "**A Study on the Metal Tube Type Ultrasonic Motor (MTTUSM)**", European Frequency and Time Forum International Frequency Control Symposium, pp. 609-612 (2009, Besancon of France).

[20] Jwo-Ming, Jou and Kai-Lin, Huang, "Miniature Piezoelectric Motor-Trolley", Proceedings of ICAST2006:17th International Conference on Adaptive Structures and Technologies pp.380~387, (2006/10/16~19, Taiwan).

[21] Jwo-Ming, Jou and De-Yang, Dai, "A Study for the Piezoelectric Motor-Trolley Driving Way", Journal of the Chinese Society of Mechanical Engineers, Vol.27, No.6, pp.639~645 (2006, Taiwan).

[22] Jwo-Ming, Jou, "Piezoelectricity Mechanics", Chwa Science and Technology Library Co. (2003/11, Taiwan).